The Astronomical Journal, 131:1436–1444, 2006 March

DYNAMICS AND STELLAR CONTENT OF THE GIANT SOUTHERN STREAM IN M31. II. INTERPRETATION

Andreea S. Font,[1] Kathryn V. Johnston,[1] Puragra Guhathakurta,[2]
Steven R. Majewski,[3] and R. Michael Rich[4]
Received 2004 June 7; accepted 2005 July 3

ABSTRACT

We examine the nature of the progenitor of the giant stellar stream in M31 using as constraints new radial velocity measurements of stream red giant stars (presented in the companion paper by Guhathakurta and coworkers) along with other M31 data sets available in the literature. We find that the observations are best fitted by orbits that are highly eccentric and close to edge-on, with apocenter to pericenter ratios on the order of 25–30 and with apocenters at or only slightly beyond the southern edge of the current data. Among these orbits we are able to find a few that plausibly connect the stream with the northern spur or with the low surface brightness feature of high metallicity similar to that of the stream (originally reported by Ferguson and coworkers) to the east of M31's center. In the latter case, if the connection is real, then the eastern debris should lie well in front of M31, near the apocenter of the orbit. Both the width of the debris and velocity dispersion measurements imply a rough lower limit on the mass of the progenitor of $10^8\ M_\odot$. We use this limit and our orbits to discuss which of M31's satellites could be plausibly associated with the stream. In addition, we predict that the width of the stream should increase beyond the southern edge of the current data around the apocenter of the orbit and that the line-of-sight velocity dispersion should exhibit significant variations along the stream.

Key words: galaxies: evolution — galaxies: individual (M31) — galaxies: kinematics and dynamics — galaxies: structure

1. INTRODUCTION

The recently discovered giant stellar stream to the south of the Andromeda spiral galaxy (hereafter referred to as the giant southern stream in M31) is thought to be debris from the (ongoing or past) disruption of a satellite dwarf galaxy (Ibata et al. 2001a; Ferguson et al. 2002). This finding has sparked a series of follow-up observations (McConnachie et al. 2003; Ibata et al. 2004), including those presented in the companion paper by Guhathakurta et al. (2006, hereafter Paper I), as well as speculations about possible associated objects (Merrett et al. 2003, 2006; Hurley-Keller et al. 2004). Such extended debris is interesting because the dynamics are relatively simple to model (Tremaine 1993; Johnston 1998; Helmi & White 1999): the stars in debris streams are dissipationless, so the essential ingredient of these models is simply phase mixing along a single orbit. As a consequence, streams offer a potential gold mine of information about their origins, with constraints on the orbit, mass, and time since disruption of the progenitor object buried in the morphology and kinematics of the debris (see Johnston et al. [2001] for a general discussion of interpreting streams around external galaxies).

The best-studied example of satellite disruption is the Sagittarius dwarf galaxy (discovered by Ibata et al. 1994), a satellite of our own Milky Way (see Majewski et al. [2003] for a review of observational work). Models for the Sagittarius dwarf's debris have not only told us about its own history (e.g., Johnston et al. 1995; Velázquez & White 1995; Ibata & Lewis 1998; Gómez-Flechoso et al. 1999; Law et al. 2005) but have also offered insights into the shape of the Milky Way's potential (Ibata et al. 2001b; Johnston et al. 2005). Information extracted from debris around other galaxies is in general much more limited because the data sets are usually restricted to surface photometry, with no practical way to measure distance or velocity variations. The M31 stream is the first example of debris around another galaxy that can be studied in more detail because it is close enough that the individual giant stars can be resolved, distances can be estimated from the tip of the red giant branch (McConnachie et al. 2003), and velocities can be obtained from spectra (Paper I; Ibata et al. 2004). Such studies have already led to specific estimates of the orbit of the progenitor and limits on M31's mass (Ibata et al. 2004). A more detailed investigation of the nature of the progenitor is now possible with recently acquired data on the width and the velocity dispersion of the stream.

In this paper we revisit the constraints on the orbit of the progenitor (§ 2) and estimate what limits can be placed on its mass (§ 3) and which M31 objects (and other low surface brightness features) could be plausibly associated with the stream, given these estimates (§ 4). We summarize our conclusions in § 5.

2. CONSTRAINTS ON THE ORBIT

2.1. *Observational Constraints*

The available spatial and velocity information on the giant southern stream and satellites of M31 is discussed in this section and summarized in Table 1. In this, these data are used to set up the initial conditions and to serve as additional constraints for our orbit integration.

Our own observations (Paper I) provide two important constraints on the orbit of the giant southern stream:

1. The mean radial velocity in the field a3 is -458 km s^{-1} relative to the Sun, which translates to $v_{\rm rad} - 158$ km s^{-1} with respect to M31.

[1] Van Vleck Observatory, Wesleyan University, Middletown, CT 06459.
[2] UCO/Lick Observatory, Department of Astronomy and Astrophysics, University of California, Santa Cruz, CA 95064.
[3] Department of Astronomy, University of Virginia, Charlottesville, VA 22903.
[4] Department of Physics and Astronomy, University of California, Los Angeles, CA 90095.

TABLE 1

Positional, Line-of-Sight Distance, and Radial Velocity Data with Respect to M31 for Fields along the Giant Southern Stream and Satellite Galaxies

Field/Name	ξ (deg)	η (deg)	d (kpc)	v_{rad} (with respect to M31) (km s^{-1})
a3	+1.077	−2.021	850:	−158
1	+2.015	−3.965	886	0:
2	+1.745	−3.525	877	−50:
3	+1.483	−3.087	860	...
4	+1.226	−2.653	855	...
5	+0.969	−2.264	840	...
6	+0.717	−1.768	836	−180:
7	+0.467	−1.327	829	...
8	+0.219	−0.886	780	−300:
12	−0.731	+0.891	739	...
13	−0.963	+1.342	758	...
M31	0.0	0.0	780	0
M32	0.0	−0.4	780	+100
NGC 205	−0.5	+0.4	830	+55
And VIII	0.1	−0.5	...	−204

Notes.—Colons indicate an uncertain measurement, and ellipses indicate missing data. The positions and line-of-sight distances for fields 1–13 are from McConnachie et al. (2003), and the radial velocities for fields 1, 2, 6, and 8 are from Ibata et al. (2004) and Lewis et al. (2004). The radial velocity for field a3 is from our data (see Paper I); for the distance to this field, an intermediate value between fields 4 and 5 is adopted (see text for details). The data for the satellites M32 and NGC 205 are from Mateo (1998); the data for And VIII are given by Morrison et al. (2003). Here (ξ, η) are the central coordinates of And VIII, a feature that is found to extend approximately 10 kpc parallel to the semimajor axis of the M31 disk and about 2 kpc along the semiminor axis, respectively. A distance of 780 kpc is adopted for M31 as in McConnachie et al. (2003) for consistency with the distance determinations of their stream fields.

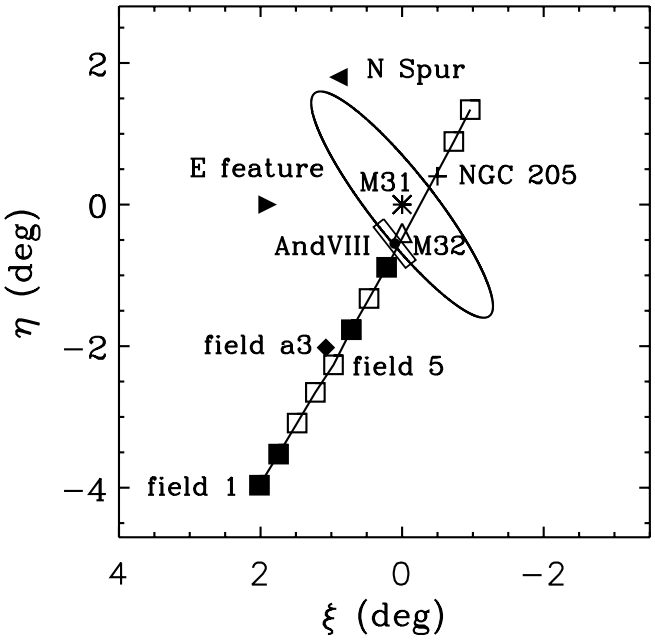

Fig. 1.—Positions of the stream fields, M31 satellite galaxies, and other stellar features expressed in standard coordinates ξ and η. The filled squares and the diamond denote the fields for which radial velocity information is available (see Table 1). The ellipse delineates the limit of the visible disk of M31 with a semimajor axis length of 2° (see Ferguson et al. 2002). The line connecting the stream fields traces the extent of the giant southern stream, as detected so far. The eastern high-metallicity feature lies roughly at $\xi \sim 2°$ and $\eta \sim 0°$. The narrow rectangular strip delineates And VIII, a feature that is found to extend approximately 10 kpc parallel to the major axis of the M31 disk and about 2 kpc along the minor axis (Morrison et al. 2003).

2. The position-velocity data provide a measure of the velocity gradients both along the stream and perpendicular to it: $dv/dr_{\parallel} \sim -0.5$ km s^{-1} arcmin^{-1} and $dv/dr_{\perp} \sim +0.6$ km s^{-1} arcmin^{-1}, respectively. There is considerable uncertainty, however, in the determination of these slopes due to possible confusion between stream stars and those in the smooth M31 halo, as well as small number statistics.

Our data are complemented with information from a few other studies:

1. McConnachie et al. (2003) have estimated line-of-sight distances as a function of sky position for several fields along the giant southern stream. These imply that the stream sweeps from over 100 kpc behind M31 at the point furthest from the disk in the south (field 1) to 30 kpc in front of the disk in the north (field 13; see Table 1 for a summary).

2. Ibata et al. (2004) and Lewis et al. (2004) find that the southernmost tip of the stream is nearly at rest with respect to M31 (i.e., moving at the systemic velocity of M31), whereas the stream in the vicinity of the disk reaches a radial velocity of about −300 km s^{-1} with respect to M31. This difference of about 165 km s^{-1} in radial velocity between fields 1 and 6, subtending about 3° across the southern part of the stream (see Fig. 1 of Ibata et al. 2004), implies a velocity gradient of $dv/dr_{\parallel} \simeq -0.9$ km s^{-1} arcmin^{-1}, in rough agreement with the observed value within our field a3 (see Fig. 8 of Paper I).

Figure 1 illustrates the positional data of the giant southern stream fields and of M31's satellite galaxies. The spatial and velocity information together offer a general picture of the dynamics of the stream. The southern part of the stream is located behind the disk (as seen from our location) and is traveling generally toward M31 along almost a straight line path, with an inclination of about 60° with respect to the line of sight (McConnachie et al. 2003); this implies that the orbital plane must be inclined by at least $i = 30°$ to the plane of the sky and cannot be face-on.

Indeed, the linearity of the stream in the sky and its proximity to the center of M31 in field 8 suggest that the inclination[5] of the orbital plane is closer to $i = 90°$ (i.e., edge-on), since any curvature of the orbit would otherwise be apparent. In addition, the strong velocity and distance gradients and the large range in measured separations from M31 along the stream indicate that the orbit is eccentric. Finally, the linearity of the stream suggests that its orientation in space corresponds to the direction of motion, with negligible motion perpendicular to it. Hence, the full space velocity relative to M31 can be estimated at each point along the observed stream to be on the order of $v_{rad}/\cos(60°) = 2v_{rad}$. Since the southernmost part of the stream has a radial velocity close to zero with respect to M31, this would imply that this location is near or even coincides with the apocenter of the orbit.

In addition to the above data, there are two other "features" that stand out in the star-count and metallicity maps:

1. A high-density stellar feature is observed near the northeastern end of the disk major axis (Ferguson et al. 2002) and is known as the "northern spur." Its metallicity is higher than that of the disk and the neighboring halo. The origin of this feature is

[5] Throughout the paper, the inclination i is used to denote the angle between the orbital plane and the plane of the sky. An inclination angle of $i = 0°$ corresponds to the case in which the normal vector $\boldsymbol{n}$ to the orbit—defined by the direction of the total angular momentum of the orbit—is oriented toward the observer.

still unknown. It has been hypothesized to be either part of the giant southern stream or an extension of the disk (Ferguson et al. 2002; Merrett et al. 2003). In the latter case, this would imply a very significant warp of the disk.

2. A high-metallicity feature was noted by Ferguson et al. (2002) immediately to the south of the northeastern half of the disk. Surprisingly, the metallicity of this feature is comparable to that of the giant southern stream. It also appears to be higher than the overall metallicity of the northern spur (see Fig. 5 of Ferguson et al. 2002), although we caution that it is possible that a similar high-metallicity component may be present in the northern spur but be hard to disentangle from the large number of typical (i.e., lower metallicity) halo stars in the region. Since it lies more or less east of M31's center, we refer to it as the "eastern high-metallicity feature."

The peculiarities of these two features raise the question of whether they may be related to the orbit of the giant southern stream. Unfortunately, no distance or velocity measurements are available yet for either of these features, and they are therefore not included as constraints in the orbit integrations. However, their possible connection with the stream, as inferred from our orbit integrations, is discussed later (§ 2.3).

2.2. *Test Particle Orbits*

We now integrate test particle orbits in a static M31 potential in order to find the general characteristics of those that could be consistent with the data summarized in Table 1. The form of the potential contains three components: a dark halo,

$$\Phi_{\rm halo} = v_{\rm halo}^2 \log\left(r^2 + d^2\right), \tag{1}$$

a Miyamoto & Nagai (1975) disk,

$$\Phi_{\rm disk} = -\frac{GM_{\rm disk}}{\sqrt{R^2 + \left(a + \sqrt{z^2 + b^2}\right)^2}}, \tag{2}$$

and a Hernquist (1990) bulge,

$$\Phi_{\rm bulge} = \frac{GM_{\rm bulge}}{r + c}. \tag{3}$$

For the parameters in relations (1)–(3), we adopt the same values that Bekki et al. (2001) used to obtain a reasonable fit to the M31 data: $d = 12$ kpc, $v_{\rm halo} = 131.5$ km s^{-1}, $M_{\rm disk} = 1.3 \times 10^{11}\ M_\odot$, $a = 6.5$ kpc, $b = 0.26$ kpc, $M_{\rm bulge} = 9.2 \times 10^{10}\ M_\odot$, and $c = 0.7$ kpc. With these parameters the rotation speed reaches 260 km s^{-1} at a radial distance of 26 kpc, in good agreement with the observations of M31 (e.g., Kent 1989) and the recent global mass constraint derived by Ibata et al. (2004). Note that relation (1) assumes that there is no flattening of the halo potential. Present observational data are insufficient to probe the extent to which the M31 halo may be flattened. However, given that the stream data are confined to less than one orbital period, we expect the effects of weak or moderate flattening to be minimal (see also Merrett et al. 2003).

Throughout the remainder of this paper we denote with (x, y) the coordinates in the plane of the sky [aligned with the angular coordinates (ξ, η)] and z along the line of sight. The orbit integrations are performed in a coordinate system having two axes aligned with M31's disk (denoted $x_{\rm M31}$ and $y_{\rm M31}$) and a third one, $z_{\rm M31}$, perpendicular to the disk. We choose to start our orbit integrations from a location near the center of the giant southern stream, where both spatial and velocity data are available. Thus, we choose field 5 as the starting point and assign to it the radial velocity found in the neighboring field a3, $v_{\rm rad} = v_z = -158$ km s^{-1} (this choice is reasonable both due to the proximity of these two fields and because Fig. 8 of Paper I shows that a strong gradient in the direction perpendicular to the stream, $dv/dr_\perp$, can be ruled out). Starting from field 5, we then integrate both backward and forward in time.

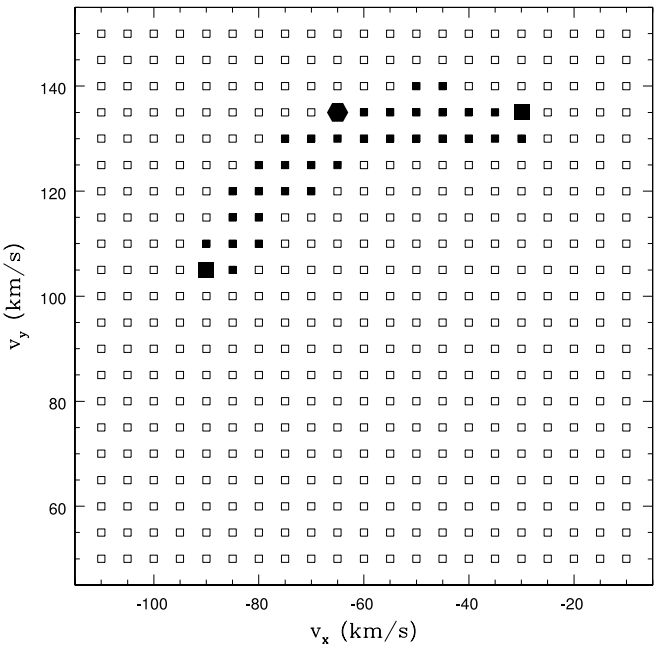

FIG. 2.—Grid of 21×21 orbits with fixed initial radial velocity, $v_z = -158$ km s^{-1}, and sampling the (v_x, v_y)-parameter space in steps of 5 km s^{-1} around the value $(-80, 132)$ km s^{-1}. Filled squares denote orbits that are found to be acceptable fits to the stream data, whereas open squares denote the rest of the orbits in the grid. Large symbols highlight the three cases chosen for further analysis: the large squares represent the two extremes of the acceptable set of orbits (i.e., orbits A and C with inclinations $i = 70^\circ$ and 115° to the plane of the sky, respectively), and the large hexagon represents a central case (orbit B, with $i \sim 90^\circ$ to the plane of the sky, i.e., an edge-on orbit).

Given the lack of data for the other two components of the velocity, v_x and v_y, we decided to construct a grid of orbits in order to constrain this parameter space. An initial inspection of the overall parameter space shows that orbits that are good fits to the data have initial conditions that cluster in the vicinity of the value $(v_x,\ v_y) = (-80,\ 132)$ km s^{-1}. Our final grid consists of 21×21 orbits, all having a fixed initial radial velocity, $v_z = -158$ km s^{-1}, and sampling the (v_x, v_y)-plane in steps of 5 km s^{-1} around $(v_x,\ v_y) = (-80,\ 132)$ km s^{-1}.

All grid orbits are shown in Figure 2 (*open squares*). Among these orbits we need to select those that fit the stream data. Given that stream data may not be accurate representations of the progenitor data (streams may deviate significantly from the progenitor's orbit), a "best-fit" method may not always be relevant. Therefore, we choose to adopt a simple accept-or-reject method by which we consider as acceptable only those orbits that pass within a series of "boxes" centered on the stream data and extending in both spatial and velocity dimensions. A reasonable choice for the size of these boxes would be on the order of the measurement uncertainties. Figure 2 (*small filled symbols*) shows the orbits accepted based on the criteria $|\Delta x| = |\Delta y| = |\Delta z| = 16$ kpc and $|\Delta v_z| = 16$ km s^{-1}. Note that we consider boxes only around fields 1–8, since fields 12 and 13 are generally difficult to fit (see a similar discussion by Ibata et al. 2004). From the set of acceptable orbits we choose three to illustrate their

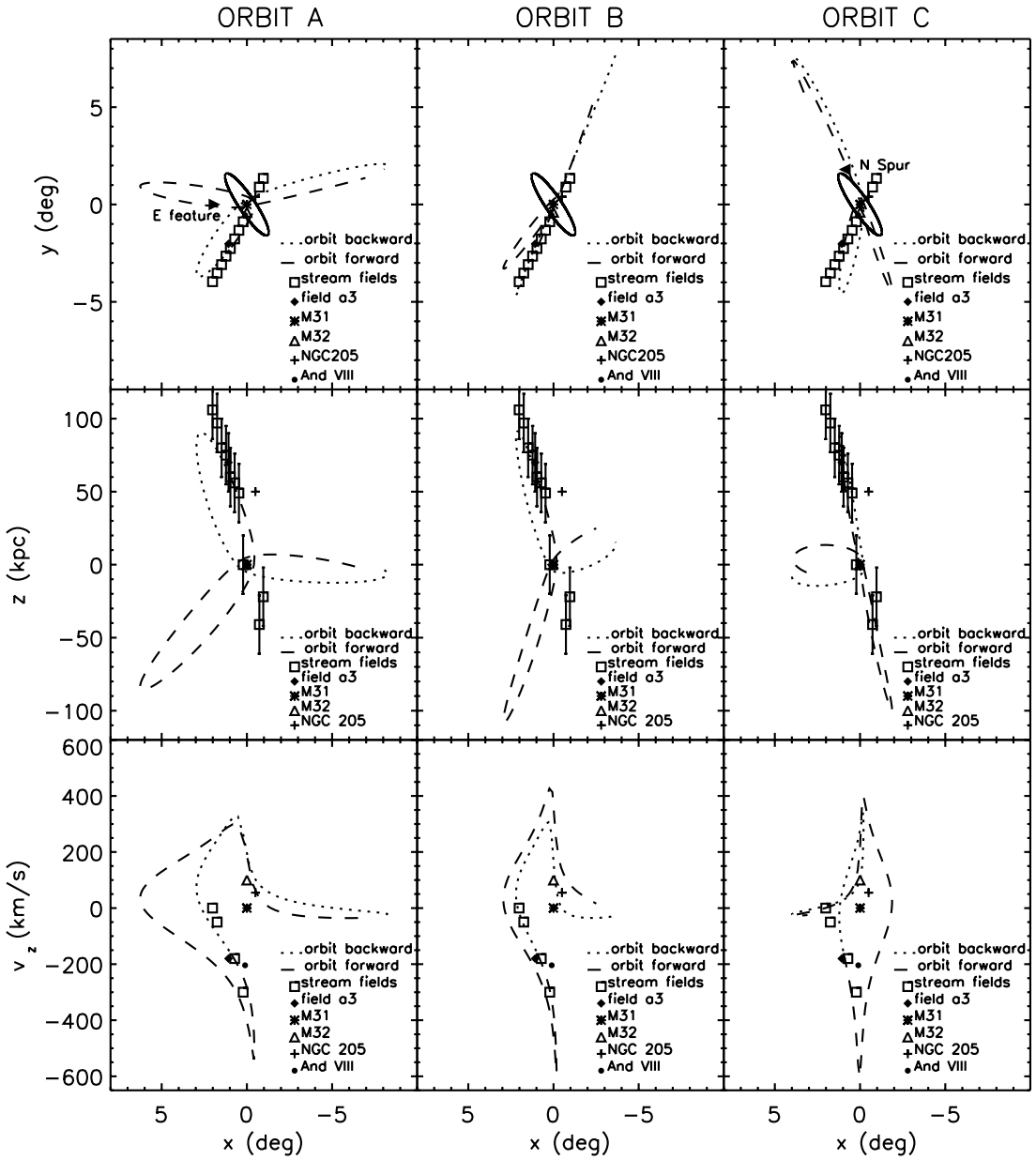

FIG. 3.—*Top panels*: (x, y)-projection of the giant southern stream fields, data on M31 satellite galaxies, and integrated orbits. The three columns correspond to the three selected orbits A, B, and C. The ellipse delineates the limit of the visible disk of M31 (semimajor axis of 2° or 27 kpc). *Middle panels*: Same as top panels, but showing the (x, z)-projection. *Bottom panels*: Radial velocity v_z along the orbits plotted against the x-component of the distance. The radial velocity measurements in fields 1, 2, 6, and 8 along the stream are approximate values inferred from Ibata et al. (2004).

common characteristics. These are highlighted in Figure 2 (*large symbols*). The large squares represent the two orbits with extreme inclinations out of the "acceptable" set ($i = 70°$ and $115°$) and are denoted from now on as orbits A and C, respectively. The large hexagon represents an intermediate case (edge-on to the plane of the sky; i.e., $i \sim 90°$) and is denoted as orbit B. Note that orbit B satisfies the most stringent conditions; for example, by reducing the box sizes to $|\Delta x| = |\Delta y| = |\Delta z| = 15$ kpc and $|\Delta v_z| = 15$ km s^{-1}, the set of acceptable orbits consists of only a few centered around orbit B. Not surprisingly, the orbits found by us to be good fits to the stream data are similar to the orbits presented by Ibata et al. (2004) and Lewis et al. (2004).

Figure 3 shows orbits A, B, and C in more detail. The top and middle panels show the (x, y)- and (x, z)-projections of the stream data and the orbits; the bottom panels show the radial velocity v_z along the orbits compared with the observed values in fields 1, 2, a3, 6, and 8, as well as the data on M31 satellite galaxies. Figure 4 illustrates the three-dimensional positions of the stream fields and orbit B in the $(x_{M31}, y_{M31}, z_{M31})$ system of coordinates.

Note that we give more weight in our fit to radial velocities than to line-of-sight distances because the latter are more susceptible to systematic errors, e.g., contamination of the tip of the red giant branch region by intermediate-age asymptotic giant branch stars and metallicity effects. The uncertainty in *relative* distance between M31 and the stream fields may be larger than the 20 kpc distance error quoted by McConnachie et al. (2003) because of differences between the stellar populations of the stream and the central region of the galaxy. Finally, field 8 has the weakest contrast of the stream against the main body of M31, and this may be problematic for both distance and radial velocity measurements (e.g., see Fig. 1 of Ibata et al. 2004).

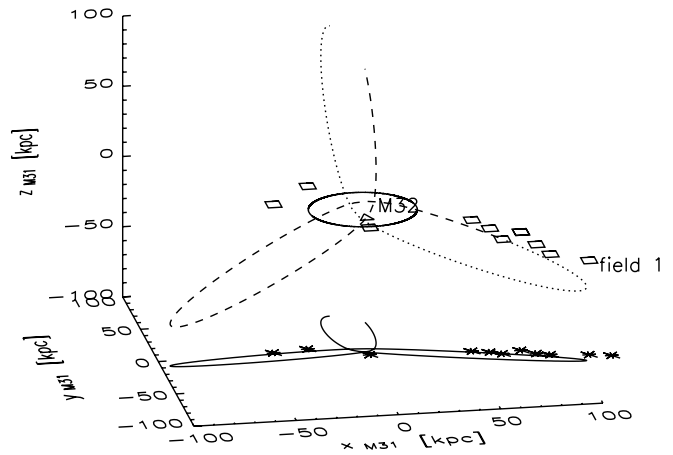

FIG. 4.—Three-dimensional position of the giant southern stream and orbit B (see § 2) in the system of coordinates ($x_{M31}, y_{M31}, z_{M31}$). The dotted line denotes the orbit integrated backward in time, and the dashed line denotes the orbit integrated forward in time. The positions of M32 and field 1 are indicated. The solid line and asterisks illustrate the projection of the orbit and the stream field positions onto the plane of the M31 disk, respectively. The ellipse represents the visible disk of M31, a circle of radius 27 kpc in the (x_{M31}, y_{M31})-plane.

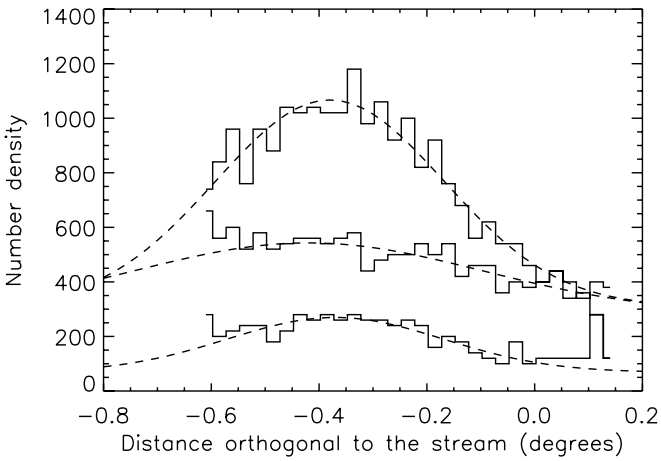

FIG. 5.—Distribution of stars at various locations along the stream, as measured by McConnachie et al. (2003). The top histogram corresponds to fields 6 and 7, the middle to fields 4 and 5, and the bottom to fields 1–3. The dashed lines represent the best Gaussian fits to the data. The width of the stream (which is proportional to the standard deviation of the Gaussian) does not vary significantly along the southern fields.

2.3. *Implications*

Several orbits provide good fits to the data, a reflection of the limited nature of the observational constraints. However, we find orbits with a small range of inclinations to the plane of the sky ($i = 70°$–$115°$) to fit the giant southern stream data well. All orbits that fit the data share the common characteristics of a fairly high eccentricity and approximately the same apocenter. These are a consequence of the imposed constraints on the orbit: the measurement of zero velocity (relative to M31) at the southern end of the stream (field 1), coupled with the large range in line-of-sight distances, which tells us that the orbit is inclined to the line of sight, implies that field 1 must be near apocenter. This working hypothesis is capable of being further verified or falsified by observations. If it holds true, then the stream, as seen in projection, should turn around on itself at or slightly beyond field 1.

Given the spatial and velocity constraints imposed by the data, we also conclude the following from inspection of Figure 3:

1. It is generally difficult to fit the northern part of the stream (i.e., fields 12 and 13). In order to fit these fields one needs a large initial velocity; however, this would increase the eccentricity and apocenter radius of the orbit, rendering it inconsistent with the zero line-of-sight velocity measured in field 1.
2. We obtain a subset of orbits that pass close to the northern spur feature (e.g., orbit C). Unfortunately, no velocity measurements are available at the moment in the northern spur that could confirm or rule out this association. Note that before full spatial data and any radial velocity were available, Merrett et al. (2003) proposed an orbit that appears to match both the stream and the northern spur. This orbit can now be ruled out because it has a turning point around field 6 in the stream, a location that is much closer to M31 than the current detections in field 1. Also, a turning point in field 6 implies a line-of-sight velocity relative to M31 at that location close to zero, which is inconsistent with the current velocity measurements in adjacent fields.

Among all orbits that fit the data, orbit A coincides, at least in projection, with the eastern high-metallicity feature. This feature, located at $\xi \sim 2°$, $\eta \sim 0°$ in Figure 5 of Ferguson et al. (2002), can be either roughly along the postpericenter part of the orbit or just before the next pericenter of the orbit. The possible association with either of these two parts of the orbit can be probed only by future velocity measurements in this region. If the eastern high-metallicity feature and the giant southern stream are indeed associated, we can predict line-of-sight distances and radial velocities along this feature based on the orbit determined in § 2.2. As can be inferred from Figure 3, this feature is expected to lie at a distance of ∼100 kpc from M31 and in front of M31 as seen from our location.

3. CONSTRAINTS ON THE PROGENITOR MASS AND DEBRIS AGE

3.1. *Stream Width, Length, and Luminosity*

Simple intuition tells us to expect debris from more massive satellites to produce wider debris streams that spread more rapidly along the orbit with time. Johnston et al. (2001) present simple analytic scalings for the width and length of debris streams, assuming that the progenitor is a hot stellar system. In this section we use these ideas to discuss possible limits on the characteristics of the progenitor.

Based on their star-count data, McConnachie et al. (2003) suggest that the giant southern stream is fanning out toward the southern part of the stream. Numerical simulations show that the stream is indeed expected to fan out toward the apocenter of the orbit (in this case, toward field 1). To test this expectation, we have estimated the width of the stream by fitting Gaussian functions at various points along the stream to the density count data of McConnachie et al. (2003). These fits are presented in Figure 5. Our results do not show a significant outward increase in the standard deviation of the Gaussians fitted to the stream, although the counts are so low in the outer fields that we feel this cannot yet be ruled out.

Given the uncertainties in the other fields, we estimate the width of the stream containing 80% of the luminosity (following Johnston et al. 2001) from the combined fields 6 and 7 to be $w = 2.5\ \sigma \simeq 0.^{\circ}5$, or, assuming an average distance $d = 833$ kpc, $w \simeq 7.5$ kpc; the combined average distance of these two fields from the center of the galaxy is $R \approx 58$ kpc. These parameters can then be used to put some limits on the mass of the progenitor satellite at the time of disruption (see a similar analysis in Johnston

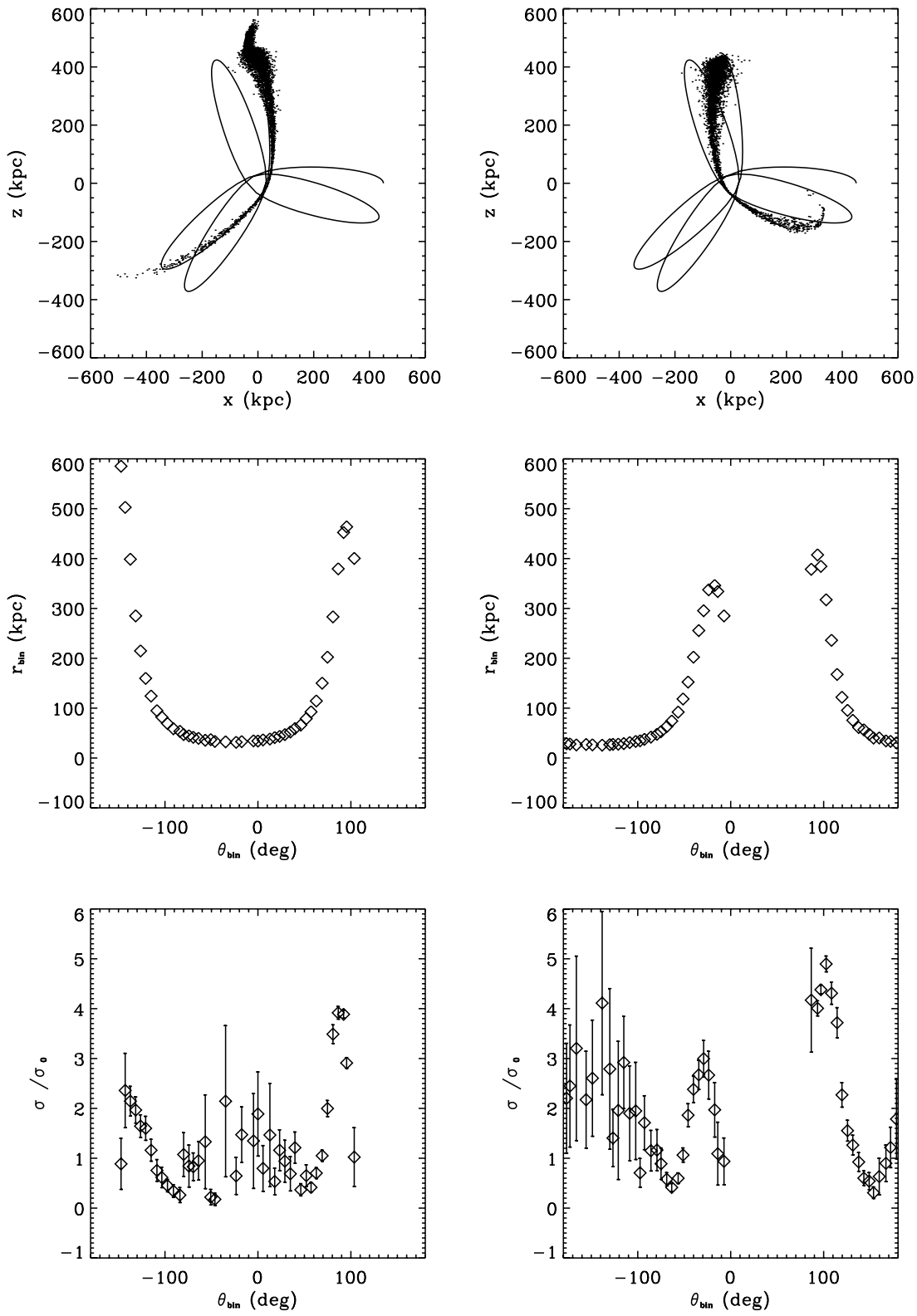

FIG. 6.—Results of an *N*-body simulation of a stellar stream moving in a highly eccentric orbit, similar to that of the orbits determined in § 2. The left and right panels correspond to the trailing and leading portions of the stream, respectively. *Top*: Positions of test particles in the orbital plane at apocenter. The solid line shows the orbit of the satellite prior to that time. *Middle*: Distance from the center of the parent galaxy plotted against the azimuthal angle θ along the giant southern stream. *Bottom*: Radial velocity dispersion with respect to the center of the parent galaxy in units of the central dispersion of the satellite, σ_0, plotted versus the azimuthal angle θ along the stream. The model suggests that, along a stellar stream moving on a highly eccentric orbit, the velocity dispersion may vary drastically relative to that of the progenitor galaxy.

et al. 2001). If the progenitor were a hot stellar system, the measured fraction, $s \equiv w/R \simeq 0.13$, is related to the mass m of the satellite through the relation $s = \left\{Gm/\left[(v_{\rm circ})^2 R_{\rm peri}\right]\right\}^{1/3}$. Given that $v_{\rm circ} = 260$ km s^{-1} and $R_{\rm peri}$ is in the range 3–4.5 kpc for our accepted orbits, one can estimate the mass of the satellite prior to the disruption from which the debris came: $m \sim (1.0\text{–}1.6) \times 10^8\ M_\odot$. From the luminosity of the stream so far detected, $L = 3 \times 10^7\ L_\odot$ (Ibata et al. 2001a), this gives mass-to-light ratios of 3.5–5.2, which are marginally consistent with those inferred from observations of nearby *dwarf elliptical* galaxies. The low mass-to-light ratio may be indicative of the nature of the progenitor. However, we caution that this ratio is rather uncertain: the progenitor may not be completely disrupted, or the observed luminosity may not be representative for the entire stream, as we have implicitly assumed. Also, for a system of similar mass with some rotation, the associated streams would be thinner, in which case these are lower bounds on the mass and mass-to-light ratios of the progenitor. These derived constraints on the progenitor's properties are similar to those found by Ibata et al. (2004).

In addition, the time t taken for the observed debris to spread along the orbit can be estimated from its observed angular extent Ψ around the parent galaxy. Johnston et al. (2001) write an expression, most valid for mildly eccentric orbits, that uses $\Psi/2\pi$ directly as an estimate of the fraction of the orbit covered with debris. Since our orbit is highly eccentric we adapt their equation (5), replacing $\Psi/2\pi$ with $\Delta t/T_\Psi$, where Δt is the time taken to travel Ψ along the orbit and T_Ψ is the azimuthal period:

$$\frac{\Delta t}{T_\Psi} \simeq 4s \frac{t}{T_\Psi}. \tag{4}$$

From our test particle orbits we find $\Delta t = 0.18\text{–}0.21$ Gyr, and hence the time since disruption for the giant southern stream is $t = 0.35\text{–}0.4$ Gyr. In conclusion, our results suggest that the giant southern stream in M31 is very young (less than an orbit old; for this orbit, the azimuthal periods for the accepted orbits are $T_\Psi \simeq 1.65$ Gyr and the radial orbital periods are $T_R \sim 1.45$ Gyr). This result is also supported by the visual appearance of the stream: the stream is young enough to be plainly visible as an overdensity in star counts (Johnston 1998).

3.2. *The Coldness of the Stream*

In Paper I the intrinsic line-of-sight velocity dispersion of the giant southern stream in field a3 was constrained to be $\lesssim 23$ km s^{-1}. What can be inferred from the coldness of the stellar stream?

Helmi & White (1999) demonstrate that the dispersion in debris should decrease over time. However, since the giant southern stream is very young, we do not expect dynamical cooling to be significant yet. Also, it has not had sufficient time to be significantly heated by tidal interactions with dark matter substructure in the halo (Johnston et al. 2002b). Rather, the velocity dispersion is expected to vary most significantly in an oscillatory manner as a function of radial orbital phase (a result also obtained by Helmi & White 1999).

Based on the orbit determined in § 2.2, we can make some general comments about the phase-space dependence of the giant southern stream. As discussed before, several arguments suggest that the orbit of the stream is highly eccentric. The orbits presented in Figure 3 have apocenter/pericenter ratios in the range $R_{\rm apo}/R_{\rm peri} \sim 25\text{–}30$. In Figure 6 we show the result of an N-body numerical simulation of a stellar stream moving in an orbit of high eccentricity ($R_{\rm apo}/R_{\rm peri} \sim 15$) as an illustration of the trends expected to occur along eccentric orbits; this is "model 4" in the numerical simulations of Johnston et al. (2002a). Figure 6 (*top panels*) shows the position in the orbital plane of the stellar debris in both the trailing (*left*) and leading (*right*) portions of the stream. The middle panels show the distance from the center of the parent galaxy versus the azimuthal angle θ along the stream. The bottom panels show the radial velocity dispersion (with respect to the parent galaxy) in units of the central dispersion of the satellite, σ_0, versus the azimuthal angle θ along the stream. Note that because the orbital plane of the stream is almost edge-on to our line of sight, we expect the observed radial velocity dispersion (i.e., along the line of sight) for fields 2–8 in the giant southern stream to exhibit effects similar to those of the radial velocity dispersion with respect to the parent galaxy in the simulations. The parameters are calculated as averages over all particles in uniform bins in θ.

From Figure 6 one can infer some general trends about the phase-space evolution of the debris: spikes in σ/σ_0, as large as a factor of 4–5, occur at the turning points (pericenter and apocenter), as predicted by Helmi & White (1999). Also, the stream can become very cold between the turning points, with the velocity dispersion of the stream reaching values well below the central dispersion of the satellite, as small as $\sigma/\sigma_0 \sim 0.5$. These effects are most pronounced for and appear to be generic features of more eccentric orbits (simulations with less eccentric orbits are not shown here). Therefore, these results could be even higher for the orbit of the progenitor, given that the orbits found in § 2.2 are even more eccentric than those of our numerical simulations.

Our field a3 lies between apocenter and pericenter in orbital phase along our fitted orbits, and hence, we expect the velocity dispersion of the progenitor to be at least as large as the intrinsic value estimated for the stream and possibly much greater than this. Adopting the nominal best-fit value of 15 km s^{-1} from the possible range of stream velocity dispersions (0–23 km s^{-1}), this implies that the progenitor satellite has a mass of $\gtrsim 10^8\ M_\odot$. This lower bound, admittedly a rough one given the caveats discussed above, is consistent with that set by the width of the debris on the mass of the satellite (see § 3.1).

Future velocity measurements can be used to confirm or rule out our prediction of significant variations of the line-of-sight velocity dispersion along the giant southern stream. Ibata et al. (2004) do have some velocity measurements in these fields but not in sufficient numbers to look for this effect; combining data from fields 1, 2, 6, and 8, they find a concentration of stars with a velocity dispersion of 11 km s^{-1} but with a skewed tail of velocities relative to the center of the stream with a spread much greater than this (this is possibly related to M31's smooth halo population; see Paper I).

4. DISCUSSION: THE POSSIBLE PROGENITOR

From the two independent mass estimates described above (§§ 3.1 and 3.2) we conclude that our progenitor satellite has a mass $m > 10^8\ M_\odot$, but this is only a rough lower bound. This result suggests that the progenitor is a massive dwarf galaxy. In particular, we note that although the observational data give an upper limit to the velocity dispersion of the stream, the theoretical models show that the stream's velocity dispersion provides only a lower limit to the velocity dispersion of the progenitor. Therefore, the satellite can have a velocity dispersion much larger than 23 km s^{-1}. Consistent with this result are the new measurements of the mean metallicity of red giant stars in field a3 in the giant southern stream (Paper I), $\langle [{\rm Fe/H}] \rangle = -0.5$ dex. Assuming that this value is representative for the satellite as well, and using the empirical metallicity-luminosity relation obtained in

the Local Group (Mateo 1998; Dekel & Woo 2003), this would imply an absolute magnitude $M_B = -17$ ($L_B \sim 10^9\ L_\odot$) and mass $m \approx 5 \times 10^9\ M_\odot$ for the progenitor satellite. While the metallicity-based estimates of the progenitor mass and luminosity are much greater than the lower bounds obtained from the stream width, luminosity, and velocity dispersion, it should be recognized that those lower bounds are very approximate for the reasons discussed above.

The large discrepancy between the direct estimate of the stream's luminosity (Ibata et al. 2001a; Morrison et al. 2003) and the progenitor luminosity inferred from our metallicity measurement may have an important implication. The former estimate corresponds only to the detected part of the stream—the luminosity of the *entire* stream may be much higher. This would suggest that a large portion of the stream or even its progenitor are currently invisible (or unidentified), either because a part of the stream has already faded into the background and/or the surviving portions of the satellite and stream are lost against the disk of M31. The recent identification of a possible high-luminosity feature ($L \sim 10^8\ L_\odot$) along the stream (Morrison et al. 2003) should caution us that other stream features may still remain undetected.

Several satellites that fit these mass and luminosity descriptions are aligned in projection along or in the close vicinity of the giant southern stream. The velocity information for the debris, which has become available only recently, is useful for ruling out some of these possible associations.

Based on our orbit integrations we can conclude that M32 is unlikely to be associated with the stream. Although M32 has a projected position almost coincident with the stream, its radial velocity has an opposite sign to those of the velocities of the fields in the giant southern stream. We can therefore exclude any possibility that the stream results from a *current* passage of M32. This can be clearly seen in the radial velocity plot in Figure 3 (*bottom panels*): the radial velocity starts from field a3 with a value of -158 km s^{-1} and decreases during the first passage; it becomes positive only in a subsequent passage. Several authors mention the possibility that the observed stream could be a remnant from a previous passage of M32 (e.g., Ibata et al. 2004). We believe that this is also inconsistent with the observations; if this scenario were true, a stream from the current passage should also be visible, and this is not supported by observations. NGC 205 is also an unlikely progenitor based on similar velocity arguments, as well as on the fact that its line-of-sight distance does not match our fitted orbits (see also the result of Ibata et al. 2004).

The satellite responsible for the stream should currently be located along the stream. The satellite can either be one of the surviving satellites around M31 or it could be totally destroyed. Given the relatively young age of the stream, the latter case implies that the satellite in question was destroyed only a short time ago. The recently discovered And VIII (Morrison et al. 2003) is an attractive possibility as a progenitor. Both its location and its radial velocity ($\xi \sim 0^\circ$, $\eta \sim -0.^\circ5$; $v_{\rm rad} = -204$ km s^{-1} with respect to M31) are consistent with those of the giant southern stream and of our determined orbit (see Fig. 3). Future observations need to confirm whether And VIII is a satellite galaxy or, as has been recently suggested (Ibata et al. 2004), simply a part of the stellar stream.

5. SUMMARY

From a comparison of test particle orbits with observational data we conclude that the progenitor of the M31 giant southern stream was (or is) on a highly eccentric, close to edge-on (to the plane of the sky) orbit with an apocenter-to-pericenter ratio on the order of 25–30 and an apocenter at or only slightly beyond the edge of the current data. Given these accepted orbits we estimate the mass of the progenitor to be $>10^8\ M_\odot$ from the width of the debris and the time since disruption to be 0.25 Gyr (less than one orbit). Moreover, *N*-body simulations suggest that our line-of-sight velocity dispersion limit of 23 km s^{-1} for the stream in field a3 is only a lower bound on the dispersion of the progenitor. In conclusion, our analyses lead us to expect that: (1) The stream should turn around slightly beyond the edge of field 1. (2) The stream should widen around this turning point, and the line-of-sight velocity dispersion should exhibit significant variations along the stream. (3) There are possible associations between the postpericenter part of the stream and the northern spur or the eastern high-metallicity feature. In the latter case, this eastern high-metallicity feature should lie well in front of the disk. Finally, (4) the kinematic data on And VIII are consistent with this feature being associated with the orbit of the giant southern stream.

K. V. J. and A. F.'s contributions were supported through NASA grant NAG5-9064 and NSF CAREER award AST 01-33617. P. G. acknowledges support from NSF grant AST 03-07966 and a Special Research Grant from the University of California, Santa Cruz. S. R. M. acknowledges funding by NSF grants AST 03-07842 and AST 03-07851, NASA/JPL contract 1228235, the David and Lucile Packard Foundation, and the F. H. Levinson Fund of the Peninsula Community Foundation. R. M. R. acknowledges support from NSF grant AST 03-07931.

REFERENCES

Bekki, K., Couch, W. J., Drinkwater, M. J., & Gregg, M. D. 2001, ApJ, 557, L39
Dekel, A., & Woo, J. 2003, MNRAS, 344, 1131
Ferguson, A. M. N., Irwin, M. J., Ibata, R. A., Lewis, G. F., & Tanvir, N. R. 2002, AJ, 124, 1452
Gómez-Flechoso, M. A., Fux, R., & Martinet, L. 1999, A&A, 347, 77
Guhathakurta, P., et al. 2006, AJ, in press (Paper I)
Helmi, A., & White, S. D. M. 1999, MNRAS, 307, 495
Hernquist, L. 1990, ApJ, 356, 359
Hurley-Keller, D., Morrison, H. L., Harding, P., & Jacoby, G. H. 2004, ApJ, 616, 804
Ibata, R., Chapman, S., Ferguson, A. M. N., Irwin, M., Lewis, G., & McConnachie, A. 2004, MNRAS, 351, 117
Ibata, R. A., Gilmore, G., & Irwin, M. J. 1994, Nature, 370, 194
Ibata, R., Irwin, M. J., Ferguson, A. M. N., Lewis, G., & Tanvir, N. 2001a, Nature, 412, 49
Ibata, R. A., & Lewis, G. F. 1998, ApJ, 500, 575
Ibata, R. A., Lewis, G. F., Irwin, M. J., Totten, E., & Quinn, T. 2001b, ApJ, 551, 294
Johnston, K. V. 1998, ApJ, 495, 297
Johnston, K. V., Choi, P. I., & Guhathakurta, P. 2002a, AJ, 124, 127
Johnston, K. V., Law, D. R., & Majewski, S. R. 2005, ApJ, 619, 800
Johnston, K. V., Sackett, P. D., & Bullock, J. S. 2001, ApJ, 557, 137
Johnston, K. V., Spergel, D. N., & Haydn, C. 2002b, ApJ, 570, 656
Johnston, K. V., Spergel, D. N., & Hernquist, L. 1995, ApJ, 451, 598
Kent, S. M. 1989, PASP, 101, 489
Law, D. R., Johnston, K. V., & Majewski, S. R. 2005, ApJ, 619, 807
Lewis, G. F., Ibata, R. A., Chapman, S. C., Ferguson, A. M. N., McConnachie, A. W., Irwin, M. J., & Tanvir, N. 2004, Publ. Astron. Soc. Australia, 21, 203
Majewski, S. R., Skrutskie, M. F., Weinberg, M. D., & Ostheimer, J. C. 2003, ApJ, 599, 1082

Mateo, M. L. 1998, ARA&A, 36, 435
McConnachie, A. W., Irwin, M. J., Ibata, R. A., Ferguson, A. M. N., Lewis, G. F., & Tanvir, N. 2003, MNRAS, 343, 1335
Merrett, H. R., et al. 2003, MNRAS, 346, L62
———. 2006, in Planetary Nebulae Beyond the Milky Way, ed. J. R. Walsh & L. Stanghellini (Berlin: Springer), in press (astro-ph/0407331)
Miyamoto, M., & Nagai, R. 1975, PASJ, 27, 533
Morrison, H. L., Harding, P., Hurley-Keller, D., & Jacoby, G. 2003, ApJ, 596, L183
Tremaine, S. 1993, in AIP Conf. Proc. 278, Back to the Galaxy, ed. S. S. Hold & F. Verter (New York: AIP), 599
Velázquez, H., & White, S. D. M. 1995, MNRAS, 275, L23